Journal of Membrane Science 659 (2022) 120804

Contents lists available at ScienceDirect

Journal of Membrane Science

journal homepage: www.elsevier.com/locate/memsci

Enhancing the durability and performance of radiation-induced grafted low-density polyethylene-based anion-exchange membranes by controlling irradiation conditions

Andrey S. Barbosa [a], Ana Laura G. Biancolli [a,*], Alexandre J.C. Lanfredi [b], Orlando Rodrigues Jr. [a], Fabio C. Fonseca [a], Elisabete I. Santiago [a,**]

[a] Nuclear and Energy Research Institute, IPEN/CNEN, 05508-000, São Paulo, Brazil
[b] Centre for Engineering, Modelling and Applied Social Sciences, Federal University of ABC (UFABC), 09210-580, Santo André, Brazil

ARTICLE INFO

Keywords:
LDPE
Anion-exchange membranes
Alkaline fuel cells
Radiation-induced grafting

ABSTRACT

This study presents a systematic analysis of the influence of irradiation conditions (absorbed dose, temperature, and atmosphere) on the physicochemical properties of radiation-induced grafted anion-exchange membranes (AEMs) based on low-density polyethylene (LDPE). Detailed characterization of the polymeric electrolytes shows striking effects of the irradiation conditions on the AEM properties. The LDPE films are irradiated both at room temperature (RT) and low temperature (LT, ~ −10 °C). At each temperature, samples are irradiated in air as well as nitrogen. By lowering the sample temperature from RT to LT during irradiation in air it is possible to obtain a threefold increase in the degree of grafting (DoG). The higher DoG reflects in the OH^- conductivity (σ) of the AEM irradiated at LT, which exhibits σ (T = 80 °C) = 215 mS cm^{-1}, while the sample prepared at RT and air has σ (T = 80 °C) = 127 mS cm^{-1}. Such high conductivity of the LT irradiated LDPE-AEM results in high-performance anion-exchange membrane fuel cell (AEMFC) with enhanced stability, as inferred from the time dependence of σ (T = 60 °C) measurements. The experimental results evidence that the control of both the irradiation temperature and the atmosphere diminishes the degradation effects caused by the radiation. Therefore, the present study advances the understanding of the role played by the irradiation process on the final properties of radiation-induced grafted LDPE-based AEMs and offers new possibilities to guide future developments for anion-exchange membranes.

1. Introduction

The growing need for environmentally friendly energy generation has led to the urgent pursuit of new technologies that can meet the global energy demands [1–3]. In this scenario, anion-exchange membrane fuel cells (AEMFC) have been gaining attention as a game-changer technology for clean energy generation. This device has been considered as a substitute to the obsolete and inefficient alkaline fuel cell (AFC) based on liquid electrolytes. The possibility of using earth-abundant metal-based catalysts and a less corrosive environment can reduce the device cost compared to the well-established proton-exchange membrane fuel cell (PEMFC) technology [2,4]. The advance of AEMFCs has been only possible due to the development of efficient anion-exchange membranes (AEM). Recently, such solid electrolytes have exhibited remarkable progress due to a better understanding and control of their fundamental properties [5–7].

A wide variety of materials has been suggested for the manufacture of AEMs [1,8–12]; however, the main challenge is to combine high conductivity, durability, stability, and low cost of the material [13]. Such properties are dependent on both the nature of the polymer matrix and the functional groups (charge carriers) [14], as well as the processing steps. Polyethylene (PE) is considered as a good choice of polymer matrix for AEMs due to its low cost, chemical stability, hydrophobicity, and good mechanical properties [15,16]. Among the different PEs subtypes, the low-density polyethylene (LDPE) has shown high mechanical resistance to ionizing radiation and high susceptibility to crosslink due to its high degree of branching [17]. These features make the LDPE a good candidate for AEM synthesis via

* Corresponding author.
** Corresponding author.
E-mail addresses: anabiancolli@alumni.usp.br (A.L.G. Biancolli), elisabete.santiago@usp.br (E.I. Santiago).

https://doi.org/10.1016/j.memsci.2022.120804
Received 15 May 2022; Received in revised form 3 July 2022; Accepted 6 July 2022
Available online 14 July 2022

radiation-induced grafting (RIG) [13,18–20].

In the RIG using the pre-irradiation method, the base polymer is irradiated with high-energy ionizing radiation, such as gamma-rays or electron-beam, to generate free radicals. The pre-irradiated film is, subsequently, placed in contact with a non-irradiated monomer for the grafting reaction, which promotes the incorporation of side chains via copolymerization [14,21,22]. Several reactions can take place simultaneously during the irradiation in PE, e.g., the formation of crosslinking and chain scission [23–27]. In addition, these reactions are highly influenced by factors such as absorbed dose, dose rate, processing conditions (before, during, and after irradiation), presence of additives, irradiation atmosphere (air, inert, vacuum), and irradiation temperature [26,28–30]. All these parameters affect the availability of sites for further grafting process.

In the pre-irradiation method, films are commonly pre-irradiated in air [18,31,32]. Consequently, the oxygen from the atmosphere reacts with free radicals in the polymer backbone forming peroxides and hydroperoxides [23,25,33–35]. Despite irradiation in air being easier and more accessible, the decomposition of peroxide and hydroperoxide species leads to the formation of oxygenated compounds such as ketones, carboxylic acids, alcohols, and esters that are not available for grafting reaction and can cause oxidative degradation in the polymer [24,25,34,35]. Oxidative degradation has been reported as a problem that results in the loss of mechanical properties and changes in the physicochemical characteristics of the polymer [26,35–37]. On the other hand, pre-irradiation can also be conducted in inert atmospheres, such as nitrogen or argon. In this case, free radicals are not scavenged by oxygen and are more available to react with each other to form crosslinks, which in the right proportion promotes an improvement in the polymer's mechanical and physicochemical properties [25,33,38]. The temperature effect has also been studied and it is related to the quantity of formed free radicals, as well as their decay and half-life time [37,39,40].

The use of radiation for the formation of free radicals in PEs, as well as the processing conditions under which these radicals are generated and their reactions in the backbone, were extensively investigated in the 60s [23,24,41–47]. Those studies represented well the materials of that time and were essential to understand the modifications in the PE's physicochemical properties after irradiation. However, over the last years, new PE-based materials have emerged, such as membranes, composites, and hybrids. Thus, further studies became necessary to elucidate the effects of irradiation on the final properties of these novel materials. Although LDPE-based AEMs have been synthesized via RIG since 1993 for various applications [48,49], it was only in 2017 that high performances were achieved by fuel cells using this type of material [19]. Despite being of great importance, reports relating the influence of irradiation conditions (temperature, absorbed dose, and atmosphere) on the final properties of the AEM and the influence of such parameters on the corresponding fuel cell response are rarely found. For instance, a recent work carried out in our laboratories evaluated LDPE-AEMs produced by two RIG methods and verified that differences in the microstructure of AEMs may compromise the AEMFC performance, even if they have the same molecular structure and ion-exchange capacity [32]. Another work by our group [38], with Ethylene tetrafluoroethylene (ETFE)-based AEMs, has shown that uncontrolled use of irradiation can cause significant losses in some polymer properties such as mechanical and chemical stability, leading to the degradation of the AEM. Preserving the integrity of the base-polymer backbone of AEMs synthesized via RIG is crucial to achieve AEMFCs that combine high performance and long-term durability, which is the current bottleneck of this technology.

All the processes involving RIG-AEM production - irradiation, grafting, and functionalization - have an important role in the durability, stability, and performance during the AEMFC operation [32]. In addition, microstructural modifications in the backbone during irradiation are complex and deserve attention. Specifically in LDPE, the occurrence of reactions leading to the deactivation of the generated free radicals is quite remarkable due to the polymer structural organization, marked by a large number of branches and low linearity [17]. In this context, this study comprehends a multi-technique analysis to evaluate the impacts of different irradiation parameters on LDPE-based AEM properties for AEMFC application.

2. Materials and methods

2.1. Membrane synthesis

Fig. 1 shows the methodology scheme for the AEMs preparation. The synthesis route followed a previously reported procedure [18,50,51] with appropriate modifications. In brief, LDPE films were irradiated under different irradiation conditions, such as absorbed dose (50 and 100 kGy), atmosphere (air and N_2), and temperature (room and low temperature). The copolymerization process (grafting) was carried out by using a mix of 3- and 4-vinylbenzyl chloride (VBC) as the monomer, followed by functionalization with trimethylamine (TMA) aiming at the formation of quaternary ammonium functional groups (QA).

LDPE films (Goodfellow, 25 μm) were pre-irradiated in four different conditions combining atmosphere and temperature: I) air at room temperature (RT, ~25 °C), II) air at low temperature (LT, ~ −10 °C), III) N_2 at RT, and IV) N_2 at LT. The N_2 atmosphere was obtained by placing the LDPE film in a hermetically sealed bag containing a one-way valve from where it was possible to remove the trapped gas. To eliminate the air (deoxygenation), N_2 (99.992%) was purged in the bag with open valve for 10 min. The bag was then fully filled with N_2, sealed, and deflated at least twice. Finally, the bag was filled with N_2 again, sealed, and proceeded to the irradiation process. Prior to irradiation, the bag was always checked for leaks. The low temperature, ~ −10 °C, was achieved by placing the samples on a dry ice layer during irradiation. The films were irradiated with 50 and 100 kGy absorbed doses. The absorbed doses were calculated using both the material density and the thickness, and by controlling the number of passes under the beam (10 kGy per pass). A Dynamitron Continuous Electron Beam Unit from RDI-Radiation Dynamics Inc. USA, model DC 1500/25/4 - JOB 188 with maximum energy of 1.5 MeV was used. The energy used in this study was 0.55 MeV, beam current of 5.74 mA, tray speed of 6 m min^{-1}, and dose rate of 39.97 kGy s^{-1}. The irradiated samples were stored for 24 h at −40 °C in an ultra-freezer prior to the grafting reaction.

To proceed with the grafting reaction, after 24 h of the irradiation step, films were immersed in a solution of 5% (v/v) of VBC (90%, Sigma-Aldrich, mix 3- and 4- isomers), 1% (v/v) of surfactant, 1-Octyl-2-pyrrolidone (Sigma-Aldrich), and 94% (v/v) of ultrapure water (UPW), previously deoxygenated in N_2 during 1 h, as described elsewhere [18,50,51]. The solution with the film was deoxygenated a second time for an additional 1 h, then the reactor was sealed and kept at 55 °C for 6 h. At the end of the reaction, the grafted films were removed from the reactor and abundantly washed with toluene and/or acetone until complete removal of the homopolymer impregnated on their surface. The samples were dried at RT for 5 h in a vacuum oven to remove all traces of solvent.

In the functionalization step, VBC-grafted LDPE films were immersed in aqueous trimethylamine (TMA) solution (45%, Sigma-Aldrich) and kept under stirring at RT for 24 h. The resulting AEMs were thoroughly washed with fresh UPW and kept at 50 °C for 1 h in UPW to guarantee TMA excess removal. After amination, all membranes were converted to Cl^- form by immersion in aqueous NaCl (1 M) overnight with the replacement for fresh NaCl solution at least twice. The resulting AEMs were then soaked in UPW to remove any excess Na^+ and Cl^- counterions. Finally, these AEMs were stored in UPW for further use.

The AEMs are referred according to the absorbed dose and irradiation conditions. For example, 100-LT-N_2 refers to the samples irradiated with 100 kGy, at low temperature, and in N_2 atmosphere. Grafted-only samples have the prefix "g" and irradiated films (prior to grafting step) have "film" in the name, as in the examples: g-100-LT-N_2 and 100-LT-N_2-film, respectively.

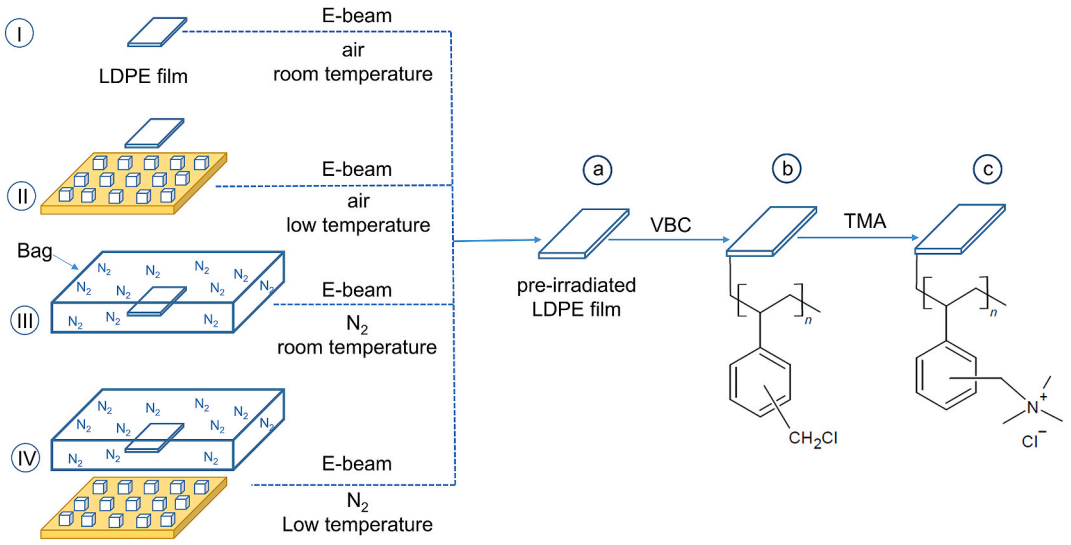

Fig. 1. Schematic representation of LDPE-g-VBC-TMA-based AEMs preparation steps: **(I–IV)** E-beam irradiation with controlled parameters, **(V)** LDPE films irradiated under different atmospheres and temperatures containing free-radicals, peroxides, and/or hydroperoxides, **(VI)** VBC-grafted film, and **(VII)** ready AEM functionalized with TMA.

2.2. Characterization of irradiated films and AEMs

The resulting membranes were characterized by measuring the degree of grafting (DoG), the water uptake (WU), and both through-plane (TPS) and in-plane swelling (IPS). The DoG was estimated by weighting the irradiated films before (m_i) and after the grafting process (m_g), as described in Equation (1). The WU of the AEMs in Cl^- form was calculated by the difference between the hydrated AEM mass (m_{hyd}) and dry AEM mass (m_{dry}) as defined by Equation (2). The thicknesses of hydrated (t_{hyd}) and dry (t_{dry}) samples for TPS determination were measured with a micrometer, while the sample areas (A_{hyd} and A_{dry}) for IPS estimation were determined with a digital caliper. The TPS and IPS (AEMs in Cl^- form) were then calculated using Equations (3) and (4).

$$DoG\ (\%) = \frac{m_g - m_i}{m_i} \times 100 \quad (1)$$

$$WU\ (\%) = \frac{m_{hyd} - m_{dry}}{m_{dry}} \times 100 \quad (2)$$

$$TPS\ (\%) = \frac{t_{hyd} - t_{dry}}{t_{dry}} \times 100 \quad (3)$$

$$IPS\ (\%) = \frac{A_{hyd} - A_{dry}}{A_{dry}} \times 100 \quad (4)$$

All measurements were repeated on three identical samples to guarantee the reproducibility of the results. All dry samples were dried in a vacuum oven at 50 °C overnight.

The ion-exchange capacity (IEC) of AEMs was determined in Cl^- form to eliminate any interference of CO_2 from the atmosphere, as described elsewhere [51]. The IEC values were obtained by potentiometric titration using an automatic titrator (Titrino 848 Plus, Metrohm) equipped with a selective Cl^- electrode.

The gel content percentage (GC) was employed to estimate the crosslinking degree of the irradiated LDPE films (prior to grafting and amination steps). The GC measurement consists of separating the soluble and insoluble phases of the polymer by Soxhlet extraction, in which the insoluble phase is an estimate of the degree of crosslinking in the sample. The GC experiments were conducted in a Soxhlet extractor adapted from ASMT D2765-16 [52]. Samples (7 × 6 cm^2) irradiated with 100 kGy were transferred to an analytical filtering paper, weighed, and placed in a Soxhlet system with xylene (Sigma-Aldrich) at 150 °C. Successive washings with xylene (6 at least) were necessary to ensure that all soluble phase was extracted to the liquid phase. All measurements were repeated on three identical samples. The GC was then calculated using Equation (5), where w_f is the final weight of the sample and w_i is the weight before extraction.

$$Gel\ Content\ (\%) = \frac{W_f}{W_i} \times 100 \quad (5)$$

Electron paramagnetic resonance (EPR) was adopted to identify and estimate the number of radicals in each irradiated sample. A Bruker EMXplus EPR spectrometer operating in the X-band was used to obtain the spectra of LDPE films irradiated with 100 kGy under the different above-mentioned conditions. Measurements were performed in films 1 h after irradiation and 24 h after irradiation. It is important to mention that the grafting step, with 3- and 4-VBC monomer, was always executed 24 h after the irradiation. All EPR measurements were carried out at low temperature using liquid nitrogen in the system to avoid the loss of free radicals during the experiment. The cavity temperature was adjusted to −40 °C ± 10 °C to simulate the sample storage environment in an ultrafreezer after irradiation. The spectra were collected with 30.0 mT sweep width, 0.1 mT modulation amplitude, microwave power of 2 mW, time constant of 81.92 ms, and 10 scans. All measurements were performed in duplicate, and the spectra were normalized by the sample mass.

Raman spectra were collected with an FT-Raman spectrometer, Bruker Optics model MultiRaman, at different stages of the preparation of the AEMs: pristine LDPE film, VBC-grafted-LDPE, and TMA-functionalized AEMs. Data were collected after 128 scans, using an excitation wavelength of 1064 nm, and laser power of 600 mW. The cross-section mapping of VBC-grafted-LDPE samples was conducted in a Raman triple T64000 (Horiba Jobin-Yvon) equipment coupled to a microscope, using a 50× Olympus objective lens, serial UIS2 – MPLN, field number (FN) 22, numerical aperture (NA) of 0.75, resolution of 0.45 μm, and working distance (WD) of 0.38 mm. The laser wavelength was 532 nm, power at sample was 2 mW, with 5 s of exposure time and 3 accumulations for each spectrum.

The mechanical properties of the irradiated-only films (100 kGy) and AEMs (Cl^- form) were evaluated by uniaxial tensile testing in an Instron 5567 instrument. The description “film” was given to the irradiated-only samples (before grafting and amination). Rectangular specimens with dimensions of 1 × 5 cm^2 were previously dried in a vacuum oven at 50 °C and the thickness of each sample was determined before each

measurement. The tensile test was carried out with a speed of 2 mm min^{-1} at RT. A minimum number of five samples was tested for each set of irradiated film or AEM.

The conductivity of the AEMs was measured using the "true OH^- conductivity" method, as described elsewhere [53–55]. Samples with 1 × 4 cm^2 area were soaked in KOH 1 M for 24 h and then placed in a 4-probe BT-112 conductivity cell (Scribner Associates). The measurements were performed in a range of 30–80 °C, with 100% of relative humidity (RH), and a constant N_2 (99.9992%) flow of 0.5 L min^{-1}. A constant potential of 0.5 V was applied to generate a current between 800 and 1000 μA responsible for the rapid decarbonation of the sample. Scanning dc sweep from −0.1 V to 0.1 V was performed using a potentiostat coupled to a Scribner Assoc. 850C fuel cell test station each 10 min, six times for each measured temperature (after 2 h conditioning at the set temperature). The resistance was obtained by fitting the linear voltage-current data and the conductivity was calculated by using Equation (6).

$$\sigma = \frac{d}{R\,x\,w\,x\,t} \tag{6}$$

where "d" is the distance between the Pt voltage sense wires (0.425 cm), "R" is the electric resistance, and "w" and "t" are the width and thickness of the hydrated AEM samples, respectively. All experiments in this section were repeated for three samples of each AEM.

2.3. Membrane electrode assembly (MEA) and fuel cell tests

Gas diffusion electrodes (GDE) were used for the AEMFC tests. The cathode catalytic layer was prepared with Pt/C (Alfa Aesar, Johnson Matthey HiSPEC 4000, 40 wt% Pt) and a homemade anion-exchange ionomer (AEI) powder (20 wt% of the total solid mass) mixed with 1 mL of water and 9 mL of propan-2-ol. The catalytic mixture was homogenized in ultrasound for 30 min, sprayed over a Toray TGP-H-60 carbon paper (GDL, non-Teflonated), and then dried in air. The AEI was prepared using ETFE powder (Fluon® Z-8820X, AGC Europe) as precursor, which was e-beam irradiated in air, at RT, with 100 kGy of radiation absorbed dose. The irradiated ETFE powder was grafted with 3,4-VBC and functionalized with TMA, following the procedure described in Ref. [50]. The obtained IEC was 2.20 ± 0.01 mmol g^{-1}. For the anodes, the catalytic layer contained PtRu/C catalyst (Alfa Aesar, Johnson Matthey HiSPEC 12100, 40 wt% Pt and 20 wt% Ru), the ETFE-AEI powder (20 wt% of the total solid mass), and Carbon Vulcan (27 wt% of the total solid mass). The same experimental procedure described for the cathode was employed for the anodes. The geometric area of the GDEs was 5.0 cm^2 and Pt loadings for all cathodes and anodes were 0.50 ± 0.03 mg cm^{-2}.

Prior to fuel cell tests, the electrodes and AEM were immersed in an aqueous solution of KOH 1 M for 1 h to convert the AEM-Cl^- into AEM-OH^- form, followed by washing with UPW to remove ions excess. The membrane electrode assembly (MEA) was placed in a Single Fuel Cell hardware supplied by Scribner Associates, USA, between two graphite plates with serpentine distribution channels (5 cm^2) and applying a torque of 5.5 N m^{-1}. A fuel cell test station 850C model, Scribner Associates - USA, was used for the electrochemical measurements. The AEMFCs were fed with H_2 (99.999%) and O_2 (99.998%). The tests were performed at 80 °C with a gas supply of 0.8 L min^{-1} for the anode and 0.5 L min^{-1} for the cathode. Each AEMFC set required different gas humidification temperatures, the exact humidification temperatures for each experiment are described in the Supplementary Information (Table S3).

2.4. Stability test

The stability tests for AEMs were performed based on the methodology developed by Dekel et al. [54–56]. Prior to experiments, samples with 1 × 4 cm^2 were soaked in a 1 M Na_2CO_3 solution for 24 h, under stirring. The solution was replaced by a fresh one 3 times to ensure the complete carbonation of the AEMs, followed by washing with UPW to eliminate the remaining ions. The thickness of the samples was measured in their CO_3^{2-} form. The membrane was placed in a 4-probe BT-112 conductivity cell (Scribner Associates) coupled to an 850C Scribner Associates Inc. The measurements were performed under pure nitrogen (99.992%) at a flow rate of 0.5 L min^{-1}. For the decarbonation of the sample, the RH was adjusted to 95% at a temperature of 40 °C. A direct current flow of 200 μA was applied by an external potentiostat, Autolab PGSTAT 302 N, aiming at replacing the carbonate ion with hydroxide ion. The resistance was obtained by fitting the linear voltage-current data from the dc sweep (−0.1 V to 0.1 V) measurements, similar to the conductivity measurement in section 2.2. The conductivity was then calculated by using Equation (6). The total conversion of the AEM was carried out in 30 h (on average) and the process was monitored by measuring the resistance of the sample every 30 min. It was assumed that the AEM was completely in its hydroxide form when the maximum conductivity was reached and there was no significant variation in the measured value. Finally, the stability tests were performed at 60 °C, RH of 80%, and applied current of 200 μA. The conductivity of the sample was collected each 30 min during 100 h of operation. The stability data was obtained from the loss in the conductivity (in percentage) as a function of time, after linear regression of the resulting data.

3. Results and discussion

3.1. Synthesis of LDPE-based AEM

Fig. 2 shows the degree of grafting (DoG) and ion exchange capacity (IEC) of AEMs irradiated with 100 kGy at different temperatures and atmospheres. The results for AEMs irradiated with 50 kGy of absorbed dose can be found in Fig. S1. As expected, samples irradiated with 100 kGy, in general, present higher DoG than the ones irradiated with 50 kGy, as follows: DoG of LT-N_2 samples: 90% - 50 kGy *vs* 116% - 100 kGy; LT-air: 83% - 50 kGy *vs* 125% - 100 kGy; RT-N_2: 57% - 50 kGy *vs* 88% - 100 kGy; RT-air: 39% - 50 kGy *vs* 43% - 100 kGy. The number of free radicals produced by the electron-beam interaction with LDPE increases with increasing radiation absorbed dose [57]. The IEC of samples irradiated with 50 kGy follows the DoG trend: 50-LT-N_2 = 2.62 mmol g^{-1} > 50-LT-air = 2.55 mmol g^{-1} > 50-RT-N_2 = 2.39 mmol g^{-1} > 50-RT-air = 1.84 mmol g^{-1} (see Fig. S1). For both set of samples (50 and 100 kGy), it is possible to notice a significant dependence of the DoG (and IEC) on the irradiation atmosphere and temperature. By analyzing samples

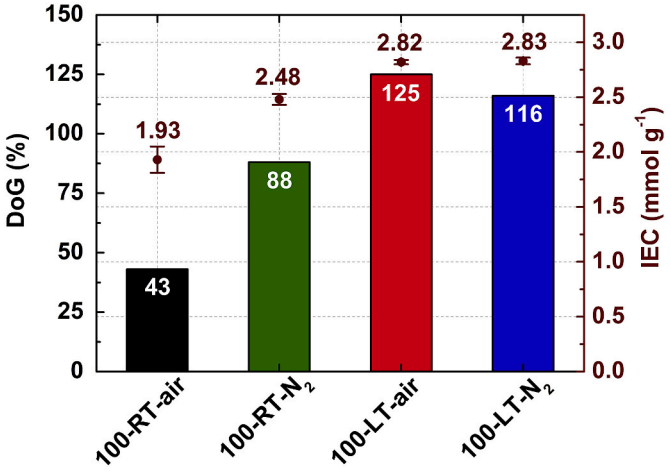

Fig. 2. Degree of Grafting (DoG) and Ion Exchange Capacity (IEC) of LDPE-based AEMs pre-irradiated under different conditions with 100 kGy of absorbed dose.

irradiated under the same atmosphere (N_2 or air), it is evident that irradiation at LT produces AEMs with higher DoG and IEC than at RT. Considering samples irradiated at RT, the ones irradiated under inert atmosphere (N_2) exhibited higher DoG (and IEC) values than the samples irradiated in air. A similar trend was previously found for AEMs based on ethylene-tetrafluoroethylene (ETFE) [38]. On the other hand, samples irradiated at LT (LT-air and LT-N_2) have shown very similar DoG and IEC, in both groups of AEMs, 100 kGy or 50 kGy, indicating that the effect of the atmosphere on the DoG (and IEC) is less pronounced at low temperature.

The observed effects of irradiation conditions shown in Fig. 2 and S1 can be understood by analyzing the reactions occurring in the LDPE film during the irradiation process, as depicted in Scheme 1 [58–62]. The irradiation of the polyethylene film leads to the formation of free radicals through the cleavage of C–H or C–C bonds, which are the initiation reactions. An alkyl radical can lead to the formation of a double bond if cleavage of the C–H bond occurs readily at the vicinal carbon. As a sequence, chain propagation reactions occur between free radicals with vinyl or vinylidene double bonds, forming new radicals [34]. In the presence of oxygen, these new radicals generate oxygenated products (ketones, carboxylic acids, esters, hydroperoxides, and alcohols). Finally, termination reactions lead to the formation of products that can generate new radicals or that are neutral/stable enough to not initiate new cycles of radical reactions [34]. These reactions are highly influenced by the intrinsic characteristics of the polymer (crystallinity, crystallite size, branching) and by the irradiation conditions (absorbed dose, dose rate, atmosphere, and temperature) [34]. For example, PEs are semi-crystalline and, therefore, have amorphous, crystalline, and interphase regions. Radiation leads to the formation of radicals in all regions of the polymer, but the radicals generated in the crystalline phase can migrate, by hopping mechanism, to the interphase and/or amorphous regions [23,63–65]. This migration is influenced by the crystallinity of the material, the path taken to the interphase, and irradiation temperature, which increases the speed of the process. Only very small molecules can reach the crystalline phase, such as H_2, H*, OH*, and He. The oxygen molecule is normally not found in this region, due to its low solubility, thus the oxidation of free radicals occurs mostly in the interphase and amorphous zones [34,66].

Scheme 1 shows the possible paths taken by radical species during and after irradiation. Irradiation can create radicals and macroradicals by hydrogen abstraction (reaction 1), leading to crosslinking (1a) and/or double bond formation (reaction 1b). By breaking C–C bonds, irradiation can also lead to chain scission (reaction 2) followed by double bond formation (reactions 2a and 2b). The irradiation in oxidative

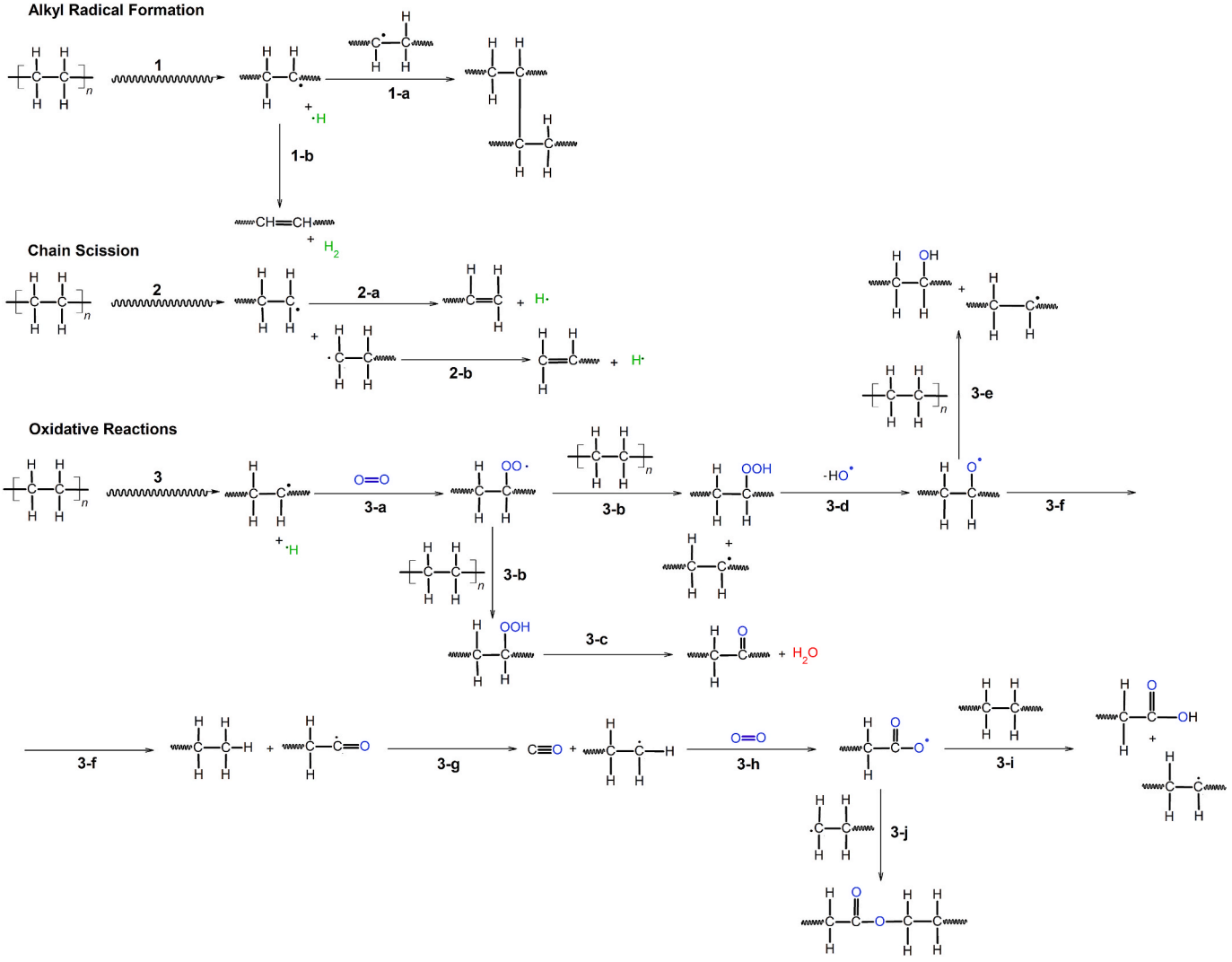

Scheme 1. Examples of reactions that can occur during the irradiation of LDPE with electron-beam. **1)** Alkyl radical formation; **1a)** crosslinking formation; **1b)** double bond formation; **2)** chain scission; **2a)** and **2b)** double bond formation; **3)** alkyl radical formation; **3a)** peroxyl radical formation; **3b)** hydroperoxide formation; **3c)** ketone formation; **3d)** hydroperoxide decomposition into alkoxyl radical; **3e)** alcohol formation; **3f)** carbonyl radical formation by oxidative degradation; **3g)** carbonyl radical decomposition; **3h)** carboxyl radical formation; **3i)** carboxylic acid formation; and **3j)** ester formation.

atmosphere generates peroxyl radicals (reaction 3a) which are known for having a rapid decay, short half-life, and for being sensitive to temperature [37,39,45,57]. These free radicals can react to form peroxides or abstract a hydrogen and form hydroperoxides (reaction 3b). They can also decompose into alkoxyl radicals to form other oxygenated species (ketones, carboxylic acid, esters) (reactions 3c-j). The oxidized radicals can recombine among the large amount of chains, since LDPE is a polymer with high branching and low linearity [57,67], or cause oxidative degradation. Oxidative degradation in polyethylene has been reported as one of the causes of chain scission in the polymer structure and consequent loss of mechanical properties [26]. Irradiation of polymers in inert atmosphere or vacuum can prevent problems caused by oxidative degradation, leaving more sites for grafting reaction, as observed in Fig. 2.

In general, the outlet temperatures of the films after irradiation in electron-beam accelerators are significantly higher than the respective inlet ones. A quick measurement using an irreversible temperature indicator paper (GEX P8003) showed a difference of over 20 °C in films irradiated with 100 kGy at RT. Such difference in temperature results from the heat generated by high-energy radiation. Considering that formed free radicals on the polymer backbone are sensitive to temperature and decay over time [37,39,45,68,69], it is reasonable to infer that the increase in temperature during irradiation can lead to an accelerated loss of free radicals. In addition, the recombination between free radicals (crosslinking reaction 1-a, Scheme 1) is more likely to happen if the polymer chains have increased mobility. These features influence the available sites for the grafting process, justifying the observed differences in the DoG of LT and RT-AEMs. Moreover, the increase in the temperature during the irradiation step promotes an increase in the oxygen diffusion in the bulk of the material, facilitating the oxidative degradation processes [26,37]. The opposite is also true and oxidative degradation is diminished at LT since the diffusion of oxygen in the structure is hampered by the low mobility of molecules [26,37]. A difference of a few degrees at the RT during irradiation can directly affect the grafting yield. Thus, a non-controlled temperature environment can lead to AEMs with distinct properties, even being synthesized by the same method. The irradiation of the film placed over a layer of dry ice (LT-AEMs) certainly minimizes the loss of free radicals normally caused by the local heat provided by the high absorbed dose of radiation, increasing the availability of sites for posterior grafting reaction. Mélot et al. [40] reported that the mobility of free radicals generated by the irradiation on polymers is insignificant at very low temperatures. The low mobility of polymer chains prevents the recombination between free radicals, minimizing the formation of crosslinking and/or non-reactive species.

Table 1 shows the IEC and the water-related parameters of the synthesized membranes, i.e., water uptake (WU), through-plane swelling (TPS), and in-plane swelling (IPS), which are important properties for dimensional stability and conductivity in AEMs. The WU of all AEMs shows a direct correlation with the IEC values, which means the water absorption capacity increases with the number of functional groups. Controlling the WU parameter is imperative since low values can minimize ionic conductivity and too high values can lead to a loss of dimensional stability, ionic conductivity, and mechanical properties of AEMs [70,71]. TPS and IPS follow exactly the same trend observed for WU.

The water-related parameters have straight relation with the IEC of each membrane since this parameter estimates the number of cationic groups that will be solvated by water. However, crosslinking also plays an important role in the hydration capacity of AEMs. Crosslinking forms a three-dimensional structure with a high steric hindrance that can hinder the water penetration in the AEM internal structures, resulting in decreased WU values [72–74]. The gel content (GC) is a measurement that can estimate the crosslinking degree of the irradiated LDPE films and, consequently, the theoretical crosslinking degree in the AEMs. Table 2 presents the GC of irradiated LDPE films (prior to grafting and functionalization steps).

Table 2 shows that the LDPE films irradiated at LT have consistently lower GC than films irradiated at RT, considering the same atmosphere. This behavior is likely to be a result of the lower recombination rate of radicals caused by the low mobility of the polymer chains at LT [26,75]. Considering the two AEMs with similar IECs, 100-LT-air and 100-LT-N_2, the slight differences in WU can be attributed to the distinct degree of crosslinking of samples. The amount of crosslinking in the samples is also influenced by the atmosphere in which LDPE films were irradiated. When the film is irradiated in N_2, there are no oxygen molecules to scavenge free radicals and they are easily recombined to form crosslinking, increasing the crosslinking concentration. In contrast, samples irradiated in oxidizing atmosphere (100-LT-air-film and 100-RT-air--film) have less crosslinking in the microstructure than the corresponding ones irradiated at the same temperature but in inert atmosphere, as it can be seen in Table 2. Oxygen during irradiation oxidizes free radicals to peroxide/hydroperoxide species. Consequently, crosslinking yield is lower because the recombination between radicals is more inhibited [38]. The GC was also measured for LDPE films irradiated with 50 kGy and a similar trend was verified, as shown in Table S2.

3.2. Electron paramagnetic resonance - EPR

Fig. 3 shows the EPR spectra obtained for LDPE films irradiated with 100 kGy under different conditions of atmosphere and temperature at two different times – 1 h after irradiation and 24 h after irradiation (samples were stored at −40 °C until the EPR measurement). The most important free radicals generated by the irradiation of PEs are the alkyl radicals (–CH_2–CH*–CH_2–), formed by the abstraction of a single hydrogen atom from the polymer backbone, the allyl radicals (-CH═CH–CH*-), and the polyenyl radicals (-$(CH═CH)_n$-CH*-), both formed by radical migration to a double bond [39,76–78]. If the irradiation process takes place in the presence of oxygen, these radicals are oxidized to form peroxyl radicals [79,80].

The spectra in the magnetic field region between 3200 and 3500 G show a multiplet that corresponds to the superposition of signals that represent a mixture of alkyl, allyl, polyenyl, and peroxyl-type radicals formed from the irradiation of the LDPE film [77,80]. The peak-to-peak height (pph) is an important information that can be quantitatively related to the population of radicals generated. Herein, the pph values are defined with respect to the most intense peak of the spectrum. The pph sequence in Fig. 3a shows a trend of 100-LT-N_2 ≈ 100-LT-air >100-RT-N_2 >100-RT-air, which is an estimate of the availability of radicals shortly after irradiation of the film (1 h). The pph values obtained for LDPE films after 24 h of irradiation are presented in Fig. 3b.

Table 1
Ion-exchange capacity (IEC), water uptake (WU), through-plane (TPS), and in-plane swelling (IPS) of AEMs(Cl^-) synthesized after different pre-irradiation conditions.

Sample	IEC (mmol g^{-1})	WU (%)	TPS (%)	IPS (%)
100-RT-air	1.93 ± 0.12	35 ± 5	3 ± 1	17 ± 5
100-RT-N_2	2.48 ± 0.05	58 ± 9	6 ± 1	28 ± 6
100-LT-air	2.83 ± 0.02	77 ± 4	12 ± 1	38 ± 1
100-LT-N_2	2.82 ± 0.03	71 ± 1	10 ± 1	39 ± 2

Table 2
Gel content of pre-irradiated LDPE films in different conditions of irradiation.

Sample	GC (%)
100-RT-air-film	52 ± 2
100-RT-N_2-film	62 ± 1
100-LT-air-film	42 ± 2
100-LT-N_2-film	50 ± 1

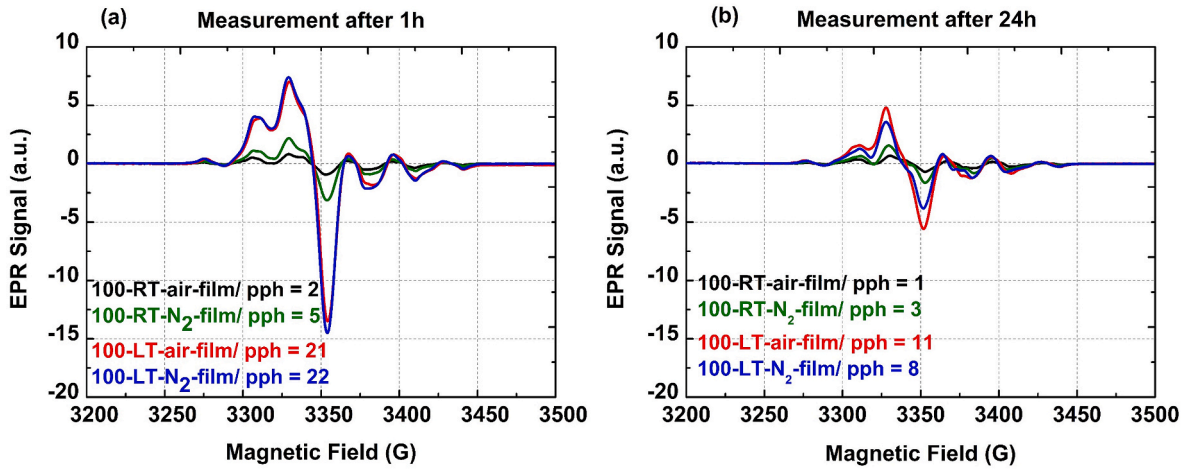

Fig. 3. EPR spectra of irradiated LDPE film in different atmospheres and temperatures. **(a)** Measurement 1 h after irradiation of the films and **(b)** measurement 24 h after irradiation of the films.

The data reveal that the estimated radical concentration follows the sequence: 100-LT-air > 100-LT- N_2 > 100-RT-N_2>100-RT-air, which is the same trend observed for the DoG values (Fig. 2). It is important to note that pph values 24 h after irradiation are lower than that in the measurement after 1 h, indicating a significant decay in the population of radicals after 24 h of storage at - 40 °C. For example, the pph of the 100-LT-air sample dropped by 50% after 24 h of irradiation. The exposition of the films to air before the grafting reaction (during storage, for example) induces the formation of peroxide/hydroperoxide species even if the alkyl, allyl, and polyenyl radicals are preferentially formed during irradiation. Such conversion of alkyl-type species, for example, to peroxide/hydroperoxide occurs in a short period of time [39].

3.3. Raman spectroscopy

The grafting reaction and functionalization step were verified by Raman spectroscopy. Fig. S2 shows the FT-Raman spectra of the pristine LDPE, the VBC-grafted LDPE, and the LDPE-based AEM. The description "g" was given to the grafted-only sample (prior to functionalization). The spectra of all final AEMs can be found in the SI, Figs. S3 and S4. The Raman spectrum of LDPE precursor film features –CH_2 bending mode at 1443 cm^{-1}, –CH_2 twisting at 1298 cm^{-1}, and C–C stretching modes at 1130 cm^{-1} [81,82]. For VBC-grafted LDPE, it is possible to identify the bands related to the VBC, such as aromatic ring stretch at 1611 cm^{-1}, meta aromatic stretch at 1000 cm^{-1}, C–Cl stretches between 600 and 800 cm^{-1}, and CH_2 wagging mode of the –CH_2Cl group at 1268 cm^{-1}

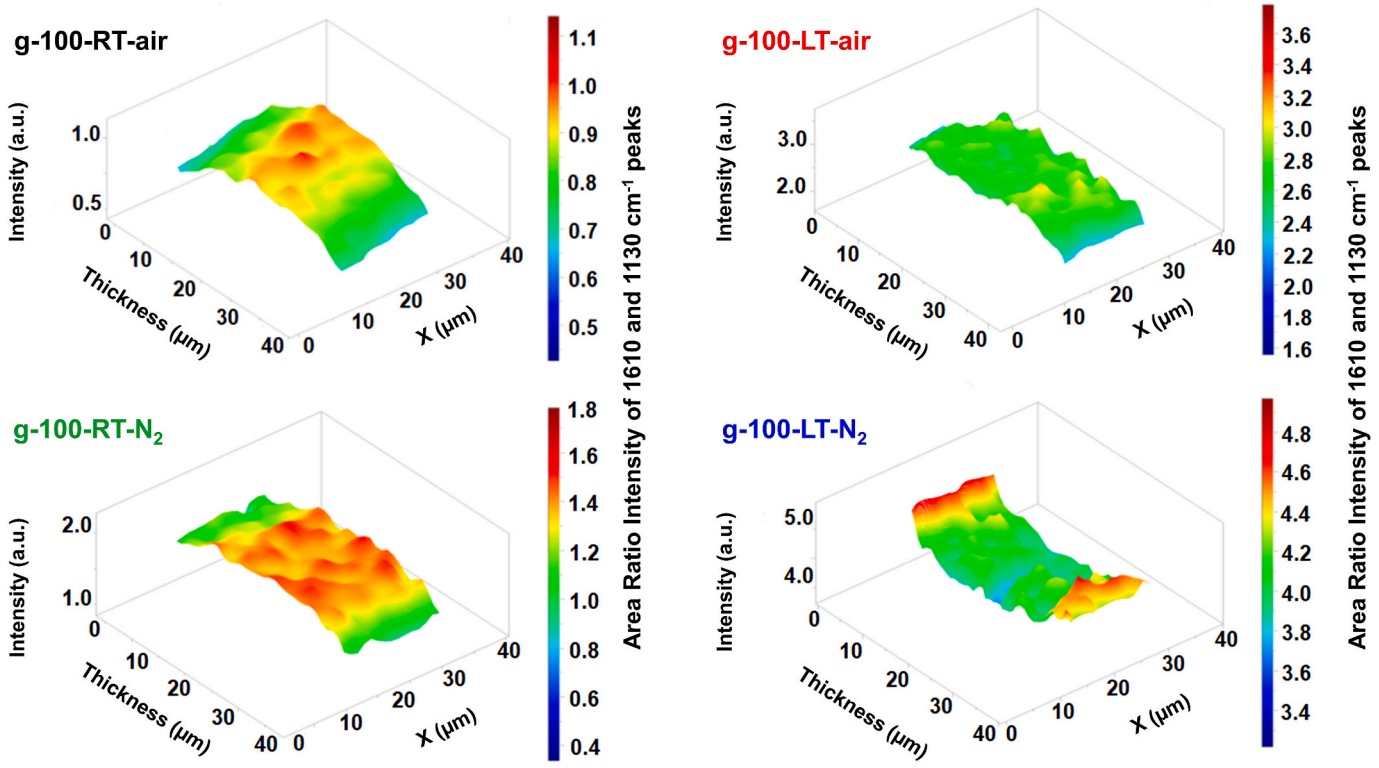

Fig. 4. Cross-sectional maps generated from the ratio between the integrated areas of the peaks 1610 cm^{-1}, from the aromatic ring of the monomer, and 1130 cm^{-1}, from the LDPE backbone.

[19,81]. For the TMA-functionalized AEMs, the amination was confirmed by the disappearance of the band at 1268 cm^{-1} and the appearance of bands referring to the trimethylammonium group, i.e. 760 cm^{-1} for symmetrical stretching of $-N^{+}(CH_3)_3$, and both 894 and 975 cm^{-1} associated with the asymmetric stretching of the group [19, 83].

The grafting homogeneity through the thickness was evaluated by mapping the cross-section of the VBC-grafted LDPE films using Raman microscopy (Fig. 4). The maps were generated by the ratio between the integrated areas of the peaks 1610 cm^{-1}, aromatic ring of the monomer, and 1130 cm^{-1} related to the LDPE backbone. It is important to mention that the intensity signal of each Raman map cannot be shown on the same scale due to the very different DoG of each sample, please see Fig. 2 for DoG values.

Fig. 4 shows that g-100-RT-air and g-100-RT-N_2 samples are more grafted in the bulk than on the surfaces. Similar graft distribution for AEM prepared under air at RT was observed by Wang et al. [19]. On the other hand, g-100-LT-N_2 shows more grafting on the surfaces than in the middle of the sample. The g-100-LT-air sample has the most homogenous grafting through the thickness of all four cases. These results indicate that the irradiation temperature has more effect on the grafting distribution than the atmosphere. The higher concentration of grafts in the bulk than on the surfaces has been attributed to the rapid diffusion of the monomer into polymer structure during the purging step with N_2 combined with the rapid deactivation of radicals on the surface of the film during the grafting process [19]. The radicals on the surface of the film are more exposed and susceptible to deactivation, so it is reasonable to infer that less grafting will occur in this region of the film, especially at high temperatures. Nonetheless, the grafting in samples pre-irradiated at LT (g-100-LT-air and g-100-LT-N_2) shows a more homogeneous distribution when compared to the ones pre-irradiated at RT. This finding reveals that the free-radicals present on the surface of the LDPE films irradiated at LT were probably preserved as much as those in the bulk. The LT certainly minimizes the recombination of free-radicals due to their low mobility, making it possible to obtain a greater distribution of grafts through the entire cross-section. Furthermore, the g-100-LT-N_2 sample showed a slightly more concentration of poly-VBC on the surfaces. This can be the result of a saturation of grafting and swelling in the LDPE bulk hindering the monomer diffusion after some reaction time.

The results suggest that the grafting homogeneity is primarily associated with free radicals decay during and after irradiation, and later related to the grafting reaction in LDPE films. The results strongly indicate that the best graft distribution can be obtained if the film is pre-irradiated at LT and in air.

3.4. Mechanical properties

The mechanical properties were evaluated by tensile stress tests performed on the pristine LDPE, the irradiated-only films, and the synthesized AEMs, as shown in Fig. 5. Measurements conducted on the irradiated-only LDPE films aimed at isolating the irradiation effects from the grafting and amination impacts on the mechanical properties of the final material.

Analyzing irradiated-only LDPE films in Fig. 5a, it can be observed that all samples present a higher elastic modulus than the pristine LDPE, confirming the material stiffening due to crosslinking [84]. The results also show that irradiation in inert atmosphere leads to higher elastic modulus when compared to the films irradiated in air at the same temperature (LT or RT). The same feature was found in a recent work for ethylene-tetrafluoroethylene (ETFE) films when irradiated in N_2 [38]. Comparing samples irradiated in the same atmosphere (air or N_2), it is observed that samples irradiated at RT have higher elastic modulus than those at LT. The elongation at break, on the other hand, seems to not be affected by the change in atmosphere, and it is more influenced by the variation in irradiation temperature. Films irradiated at LT show greater elongation at break than those at RT, regardless of the atmosphere, which can be related to the decreased extent of degradation at LT [85, 86]. Interestingly, the elastic modulus values of irradiated samples are in good agreement with the gel content results (Table 2), confirming the straight relation between the crosslinking degree and the mechanical properties.

Fig. 5b presents the mechanical properties results for the synthesized AEMs. The results are consistent with the mechanical properties of similarly prepared AEMs [19,32]. The addition of spatially bulky groups such as poly-VBC and TMA to the LDPE backbone certainly disturbs the film's microstructure [84]. This directly affects the material's crystallinity and stiffness, impacting the mechanical properties [84]. The elastic modulus in this case underwent little modification comparing the AEMs with their respective irradiated films of Fig. 5a. However, it is possible to notice that the AEMs with higher values of DoG and IEC, irradiated at LT, present the lowest values of elastic modulus among the analyzed samples. The elongation at break values remarkably decreased after grafting and amination and are very similar for all AEMs. Therefore, the impact caused on this property by the addition of functional groups does not allow the distinction of the pre-irradiation effects using this technique in the ready AEMs.

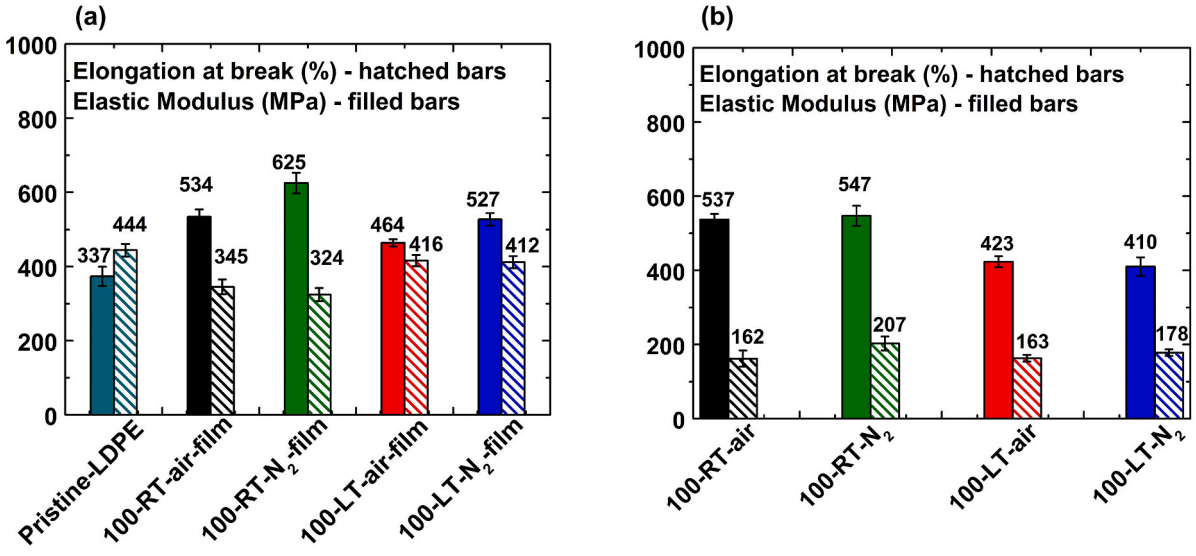

Fig. 5. Elongation at break and elastic modulus of the (a) pristine LDPE and irradiated-only LDPE films, (b) LDPE-based AEMs.

3.5. Conductivity measurement

Fig. 6 shows the temperature dependence of "true hydroxide conductivity" of the AEM in OH^- form at RH = 100%. AEM carbonation was avoided by applying a constant potential of 0.5 V during the experiment following an adapted methodology described elsewhere [53–55]. In this method, hydroxide ions are formed at the cathode by water splitting and the ions generated purge the bicarbonate species in the form of CO_2, which allows the AEM to be in its fully OH^- form [53]. The conductivity follows exactly the IEC trend. Such a feature is a consequence of the number of functional groups in each sample, which are responsible for ion conduction [70,71]. The 100-LT-air and 100-LT-N_2 AEMs have the highest IECs and conductivities (215 mS cm^{-1} at 80 °C). On the other hand, the 100-RT-air AEM presented the lowest conductivity (127 mS cm^{-1} at 80 °C) and IEC (1.93 mmol g^{-1}), while the 100-RT-N_2 AEM, with IEC = 2.48 mmol g^{-1}, displays intermediate conductivity (199 mS cm^{-1} at 80 °C).

The ionic conductivity of the synthesized AEMs follows an Arrhenius-type mechanism [87] and the activation energies are shown in Fig. S5. The OH^- mobility is strongly dependent on the inherent characteristics of the membrane, such as hydrophobicity, microstructure, and hydration [73,88,89]. Crosslinking can improve the conductivity in AEMs due introduction of phase separation between hydrophobic and hydrophilic domains that can facilitate ionic conduction; however, an excess of crosslinking can also decrease the OH^- conductivity if the hydrophobic phases act as physical barriers in the structure of the AEM [73,88,89]. The activation energy (Ea) found for AEMs ranged from 10 to 13 kJ mol^{-1}, similar to previously reported data for TMA functionalized AEMs [32,90]. Small differences in the Ea of each AEM may be a result of distinct characteristics related to hydration and microstructure.

3.6. Fuel cell tests

In order to evaluate the performance, beginning-of-life polarization curves were obtained for single fuel cells, H_2/O_2 fed (CO_2-free), using the synthesized AEMs (Fig. 7). Fuel cells were operated at 80 °C and optimized gas humidification conditions were used for each membrane to reach its ideal operation (please, see Table S3). All four curves demonstrate insignificant overpotential variations associated with the activation polarization at low current densities (<0.2 A cm^{-2}). The main difference in polarization curves is in the ohmic drop and mass transport limiting regions, which encompasses several aspects beyond the ionic conductivity of the electrolyte. The AEMFCs using 100-LT-N_2, 100-RT-N_2, and 100-LT-air AEMs present very comparable power densities (1.06–1.17 W cm^{-2}). These results are consistent with the conductivity values in Fig. 6 (199–215 mS cm^{-1} at 80 °C). On the other hand, the 100-RT-air AEM has shown the lowest power density value (0.86 W cm^{-2}) in good accordance with its conductivity (127 mS cm^{-1} at 80 °C). The water management in fuel cells plays an important role in the ion conduction mechanisms, which involves the water dragged to the anode by OH^- and back-diffusion from the anode to the cathode. A recent study [32] showed that the microstructure of AEMs directly affects ion conduction and water transportation. Thus, the observed performances can be associated with differences in conductivity, but also with the morphology of each AEM. The degree of crosslinking, chain scission extent, and oxidative degradation during irradiation lead to distinct AEM properties that influence the performance and stability of the AEMFC. Table S4 summarizes the performance results found in the literature for similar AEMs.

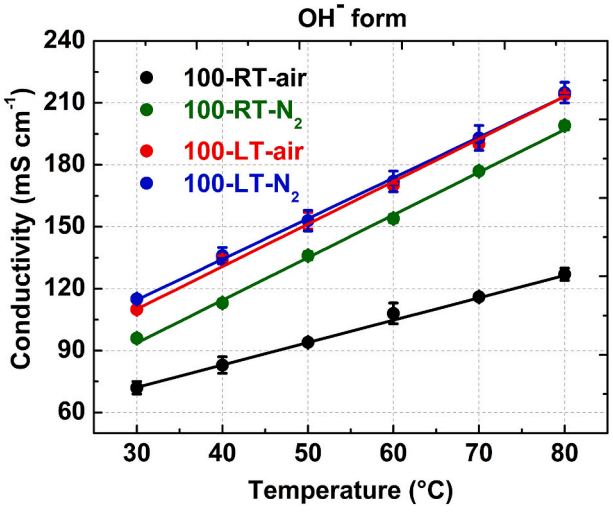

Fig. 6. Temperature dependence of the ionic conductivity at RH 100% of AEMs. Measurement of the "true hydroxide conductivity".

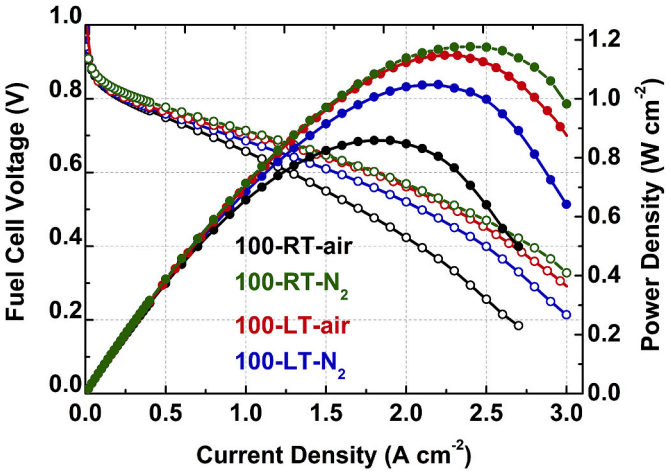

Fig. 7. AEMFCs performances at 80 °C with H_2 anode gas flow = 0.8 L min^{-1}, O_2 cathode gas flow = 0.5 L min^{-1}, both supplied unpressurised with optimal dew-point temperatures ranging from 76 to 80 °C. Catalysts: PtRu/C at the anodes and Pt/C at the cathodes. Pt loadings of 0.5 ± 0.3 mg cm^{-2}.

The set of membranes irradiated with 50 kGy (Fig. S6) showed a similar trend and comparable fuel cell performances to the AEMFCs containing the 100 kGy irradiated AEMs. The 50-LT-air membrane presented the best fuel cell performance with 1.26 W cm^{-2} of power density, followed by the membranes 50-RT-N_2 and 50-LT-N_2 (both AEMFCs reaching 1.18 W cm^{-2}). The 50-RT-air AEM presented the lowest fuel cell performance with 0.92 W cm^{-2} of power density. Therefore, it is possible to use lower radiation absorbed doses in the RIG method with little effect on the fuel cell performance. These findings also confirm that uncontrolled irradiation conditions can result in AEMs with poor physicochemical and electrochemical properties.

3.7. Stability tests

The *ex-situ* short-term stability tests were carried out using a previous protocol described elsewhere [53–55]. The decay in the true OH^- conductivity was measured as a function of time. Data was collected at 60 °C and RH = 80% during 100 h.

Fig. 8 shows the normalized results of the OH^- conductivity decay in percentage. After a linear fit of the experimental data, the stability loss rate, i.e. the loss of hydroxide conductivity was calculated in terms of percentage per hour (% h^{-1}). The OH^- conductivity loss, in Fig. 8, follows the sequence 100-RT-air > 100-RT-N_2 > 100-LT-N_2 ≈ 100-LT-air. The AEMs irradiated at LT, i.e. 100-LT-air and 100-LT-N_2, showed similar conductivity loss rates (0.10 and 0.12% h^{-1}, respectively), while samples irradiated at RT exhibited higher conductivity loss rates (0.17 and 0.22% h^{-1} for 100-RT-N_2 and 100-RT-air, respectively). Therefore,

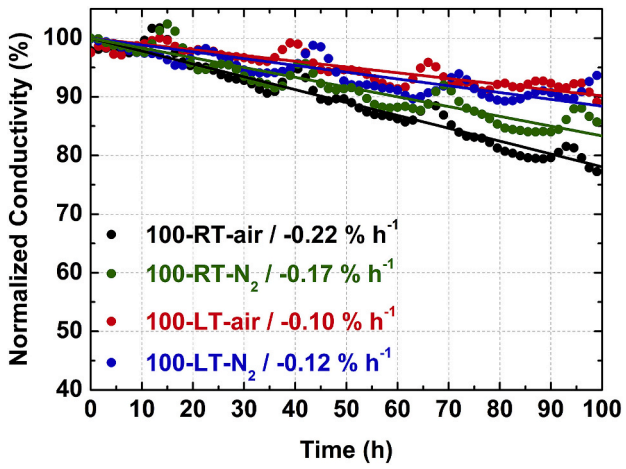

Fig. 8. Normalized true OH^- conductivity at 60 °C in RH = 80% for 100-RT-air (black line), 100-LT-air (red line), 100-RT-N_2 (green line), and 100-LT-N_2 (blue line) AEMs during 100 h. (For interpretation of the references to colour in this figure legend, the reader is referred to the Web version of this article.)

the irradiation of LDPE films at LT seems to be more favorable to produce AEMs with enhanced stability. Since all samples were grafted and functionalized using the same methodology, it is possible to attribute the AEMs stability profiles to the differences in the microstructure of the LDPE backbone caused by the distinct pre-irradiation conditions used. The extent of chain scission or the degree of crosslinking during irradiation, for example, can damage or reinforce, respectively, the films that posteriorly will generate the AEMs.

The results obtained by this study show that the LDPE-AEM short-term stability is more affected by the temperature of the pre-irradiation step than the atmosphere. Such feature is an indicative of the influence of the temperature in the acceleration of the reaction rates, mainly degradative reactions, such as chain scission [91,92], causing weakening of the polymeric structure. However, considering samples irradiated at RT, it is visible that the 100-RT-N_2 AEM has a decreased conductivity loss rate compared to the one irradiated in air, 100-RT-air AEM. Therefore, the low stability of 100-RT-air sample can be also attributed to the oxidative degradation of the polymer, which is increased if more oxygen has access to its structure [26,37,39]. Table S4 summarizes the stability results found in the literature for similar AEMs synthesized by RIG.

4. Conclusions

This study presented a systematic investigation of the effect of the irradiation conditions (absorbed dose, atmosphere, and temperature) on the physicochemical properties of radiation-induced grafted LDPE-AEMs. The irradiation conditions have a strong influence on the type, quantity, and decay of free radicals formed during and after irradiation. Such mechanisms are correlated to the physicochemical properties of resulting AEMs. The preservation of the generated radicals is crucial for successful grafting. Factors such as crosslinking degree, chain scission, and oxidative degradation in the polymer structure are relevant parameters for the final properties of AEMs. The key irradiation parameter resulting in LDPE-based AEMs with superior properties, especially regarding stability, is the irradiation of the pristine film at low-temperature (−10 °C). The detailed characterization revealed that preparing anion-exchange membranes based on LDPE that combine good electrochemical properties, stability, and fuel cell performance requires a careful control of the irradiation parameters.

CRediT authorship contribution statement

Andrey S. Barbosa: Conceptualization, Data curation, Investigation, Methodology, Visualization, Writing – original draft, Writing – review & editing. **Ana Laura G. Biancolli:** Conceptualization, Data curation, Investigation, Visualization, Writing – original draft, Writing – review & editing. **Alexandre J.C. Lanfredi:** Investigation, Resources. **Orlando Rodrigues:** Investigation, Resources. **Fabio C. Fonseca:** Funding acquisition, Resources, Writing – review & editing. **Elisabete I. Santiago:** Conceptualization, Funding acquisition, Project administration, Resources, Supervision, Writing – original draft, Writing – review & editing.

Declaration of competing interest

The authors declare that they have no known competing financial interests or personal relationships that could have appeared to influence the work reported in this paper.

Data availability

Data will be made available on request.

Acknowledgements

The authors are grateful for the support of the Center for Innovation on New Energies (CINE) - SHELL (ANP)/FAPESP grant No. 2017/11937-4, and the Brazilian Nuclear Energy Commission (CNEN). Thanks are also due to the funding support FAPESP No. 2014/09087-4 and ALGB acknowledges the funding support FAPESP No. 2019/26955-3. The authors acknowledge the financial support from International Atomic Energy Agency, research project contract: IAEA RC 23708. The authors are grateful to MSc. Djalma Batista Dias, Dr. Yasko Kodama and Radiation Technology Center, CETER-IPEN, for the support with mechanical tests, to Eng. Elizabeth S. Somessari and Eng. Heitor Gameiro Duarte for the irradiation of LDPE films, and to UFABC Multiuser Central Facility for access to the Raman equipment. FCF and EIS are fellows of the Brazilian CNPq.

Appendix A. Supplementary data

Supplementary data to this article can be found online at https://doi.org/10.1016/j.memsci.2022.120804.

References

[1] L. Shang, D. Yao, B. Pang, C. Zhao, Anion exchange membranes based on poly (ether ether ketone) containing N-spirocyclic quaternary ammonium cations in phenyl side chain, Int. J. Hydrogen Energy (2021), https://doi.org/10.1016/j.ijhydene.2021.03.059.

[2] F. Zhang, X. He, C. Cheng, S. Huang, Y. Duan, C. Zhu, Y. Guo, K. Wang, D. Chen, Bis-imidazolium functionalized self-crosslinking block polynorbornene anion exchange membrane, Int. J. Hydrogen Energy 45 (2020) 13090–13100, https://doi.org/10.1016/j.ijhydene.2020.03.046.

[3] Y. Zhang, W. Chen, T. Li, X. Yan, F. Zhang, X. Wang, X. Wu, B. Pang, G. He, A rod-coil grafts strategy for N-spirocyclic functionalized anion exchange membranes with high fuel cell power density, J. Power Sources 490 (2021), 229544, https://doi.org/10.1016/j.jpowsour.2021.229544.

[4] Z. Liu, X. Zhu, G. Wang, X. Hou, D. Liu, Novel crosslinked alkaline exchange membranes based on poly(phthalazinone ether ketone) for anion exchange membrane fuel cell applications, J. Polym. Sci., Part B: Polym. Phys. 51 (2013) 1632–1638, https://doi.org/10.1002/polb.23377.

[5] W.E. Mustain, Understanding how high-performance anion exchange membrane fuel cells were achieved: component, interfacial, and cell-level factors, Curr. Opin. Electrochem. 12 (2018) 233–239, https://doi.org/10.1016/j.coelec.2018.11.010.

[6] B. Sana, A. Das, T. Jana, Polybenzimidazole as alkaline anion exchange membrane with twin hydroxide ion conducting sites, Polymer 172 (2019) 213–220, https://doi.org/10.1016/j.polymer.2019.03.078.

[7] Z. Tao, C. Wang, X. Zhao, J. Li, M.D. Guiver, Progress in high-performance anion exchange membranes based on the design of stable cations for alkaline fuel cells, Adv. Mater. Technol. 6 (2021) 1–14, https://doi.org/10.1002/admt.202001220.

[8] E. Abouzari-Lotf, H. Ghassemi, M.M. Nasef, A. Ahmad, M. Zakeri, T.M. Ting, A. Abbasi, S. Mehdipour-Ataei, Phase separated nanofibrous anion exchange membranes with polycationic side chains, J. Mater. Chem. A. 5 (2017) 15326–15341, https://doi.org/10.1039/c7ta03967k.

[9] C. Long, Z. Wang, H. Zhu, High chemical stability anion exchange membrane based on poly(aryl piperidinium): effect of monomer configuration on membrane properties, Int. J. Hydrogen Energy 46 (2021) 18524–18533, https://doi.org/10.1016/j.ijhydene.2021.02.209.

[10] X. He, J. Zou, Y. Guo, K. Wang, B. Wu, Y. Wen, X. Zang, D. Chen, Synthesis of halogenated benzonorbornadiene monomer and preparation of self-crosslinking bisimidazole cationic functionalized benzonorbornadiene triblock copolymer anion exchange membrane, Polymer 218 (2021), 123535, https://doi.org/10.1016/j.polymer.2021.123535.

[11] Y. Wang, X. Qiao, M. Liu, L. Liu, N. Li, The effect of –NH– on quaternized polybenzimidazole anion exchange membranes for alkaline fuel cells, J. Membr. Sci. 626 (2021), https://doi.org/10.1016/j.memsci.2021.119178, 119178.

[12] T. Hamada, Y. Zhao, K. Yoshimura, A. Radulescu, K. Ohwada, Y. Maekawa, Hydrophobic effect on alkaline stability of graft chains in ammonium-type Anion exchange membranes prepared by radiation-induced graft polymerization, ChemistrySelect 6 (2021) 8879–8888, https://doi.org/10.1002/slct.202102045.

[13] R. Espiritu, M. Mamlouk, K. Scott, Study on the effect of the degree of grafting on the performance of polyethylene-based anion exchange membrane for fuel cell application, Int. J. Hydrogen Energy 41 (2016) 1120–1133, https://doi.org/10.1016/j.ijhydene.2015.10.108.

[14] G. Couture, A. Alaaeddine, F. Boschet, B. Ameduri, Polymeric materials as anion-exchange membranes for alkaline fuel cells, Prog. Polym. Sci. 36 (2011) 1521–1557, https://doi.org/10.1016/j.progpolymsci.2011.04.004.

[15] M. Zhang, H.K. Kim, E. Chalkova, F. Mark, S.N. Lvov, T.C.M. Chung, New polyethylene based anion exchange membranes (PE-AEMs) with high ionic conductivity, Macromolecules 44 (2011) 5937–5946, https://doi.org/10.1021/ma200836d.

[16] H.K. Kim, M. Zhang, X. Yuan, S.N. Lvov, T.C.M. Chung, Synthesis of polyethylene-based proton exchange membranes containing PE backbone and sulfonated poly (arylene ether sulfone) side chains for fuel cell applications, Macromolecules 45 (2012) 2460–2470, https://doi.org/10.1021/ma202492d.

[17] A.J. Peacock, Handbook Polyethylene: Structures, Properties, and Applications, New York, 2000, https://doi.org/10.1016/0167-188X(89)90104-3.

[18] L. Wang, X. Peng, W.E. Mustain, J.R. Varcoe, Radiation-grafted anion-exchange membranes: the switch from low- to high-density polyethylene leads to remarkably enhanced fuel cell performance, Energy Environ. Sci. 12 (2019) 1575–1579, https://doi.org/10.1039/c9ee00331b.

[19] L. Wang, J.J. Brink, Y. Liu, A.M. Herring, J. Ponce-González, D.K. Whelligan, J. R. Varcoe, Non-fluorinated pre-irradiation-grafted (peroxidated) LDPE-based anion-exchange membranes with high performance and stability, Energy Environ. Sci. 10 (2017) 2154–2167, https://doi.org/10.1039/c7ee02053h.

[20] M.M. Nasef, Radiation-grafted membranes for polymer electrolyte fuel cells : current trends and future directions, Chem. Rev. 114 (2014) 12278–12329, https://doi.org/10.1021/cr4005499.

[21] N.A. Qaisrani, Y. Ma, L. Ma, J. Liu, L. Gao, L. Li, S. Gong, X. Yan, F. Zhang, G. He, Facile and green fabrication of polybenzoxazine-based composite anion-exchange membranes with a self-cross-linked structure, Ionics 24 (2018) 3053–3063, https://doi.org/10.1007/s11581-017-2433-y.

[22] K.F.L. Hagesteijn, S. Jiang, B.P. Ladewig, A review of the synthesis and characterization of anion exchange membranes, J. Mater. Sci. 53 (2018) 11131–11150, https://doi.org/10.1007/s10853-018-2409-y.

[23] M. Dole, The Radiation Chemistry of Macromolecules: Free Radicals in Irradiated Polyethylene, New York, 1972.

[24] J.S.A. Singh, Radiation Processing of Polymers, Munich, 1992.

[25] I. Carpentieri, V. Brunella, P. Bracco, M.C. Paganini, E.M. Brach Del Prever, M. P. Luda, S. Bonomi, L. Costa, Post-irradiation oxidation of different polyethylenes, Polym. Degrad. Stabil. 96 (2011) 624–629, https://doi.org/10.1016/j.polymdegradstab.2010.12.014.

[26] M.A. Mulliez, C. Schilling, T.M. Grupp, Influence of irradiation temperature on oxidative and network properties of X-ray cross-linked vitamin E stabilized UHMWPE for hip arthroplasty, BioMed Res. Int. 2020 (2020), https://doi.org/10.1155/2020/2568428.

[27] A. Alsabbagh, R. Abu Saleem, R. Almasri, S. Aljarrah, S. Awad, Effects of gamma irradiation on 3D-printed polylactic acid (PLA) and high-density polyethylene (HDPE), Polym. Bull. 78 (2021) 4931–4945, https://doi.org/10.1007/s00289-020-03349-3.

[28] A. Gillis, J. Schmieg, S. Bhattacharyya, S. Li, An independent evaluation of the mechanical, chemical and fracture properties of UHMWPE cross linked by 34 different conditions, Proc. 45th Trans. Orthop. Res. Soc. (1999) 908.

[29] G. Lewis, Properties of Crosslinked Ultra-high-molecular-weight Polyethylene, 2001, https://doi.org/10.1016/S0142-9612(00)00195-2.

[30] M. Slouf, J. Mikesova, J. Fencl, H. Stara, J. Baldrian, Z. Horak, Impact of dose-rate on rheology, structure and wear of irradiated UHMWPE, J. Macromol. Sci., Part B: Phys. 48 (2009) 587–603, https://doi.org/10.1080/00222340902837824.

[31] J. Ponce-González, J.R. Varcoe, D.K. Whelligan, Commercial monomer availability leading to missed opportunities? Anion-exchange membranes made from meta-vinylbenzyl chloride exhibit an alkali stability enhancement, ACS Appl. Energy Mater. 1 (2018) 1883–1887, https://doi.org/10.1021/acsaem.8b00438.

[32] A. Laura, G. Biancolli, A.S. Barbosa, Y. Kodama, A.J.C. Lanfredi, F.C. Fonseca, Q. Rey, E.I. Santiago, Unveiling the Influence of Radiation-Induced Grafting Methods on the Properties of Polyethylene-Based Anion-Exchange Membranes for Alkaline Fuel Cells, 2021, p. 512, https://doi.org/10.1016/j.jpowsour.2021.230484.

[33] I. Ishigaki, T. Sugo, T. Takayama, T. Okada, J. Okamoto, S. Machi, Graft polymerization of acrylic acid onto polyethylene film by preirradiation method. II. Effects of oxygen at irradiation, storage time after irradiation, mohr's salt, and ethylene dichloride, J. Appl. Polym. Sci. 27 (1982) 1043–1051, https://doi.org/10.1002/app.1982.070270323.

[34] P. Bracco, L. Costa, M.P. Luda, N. Billingham, A review of experimental studies of the role of free-radicals in polyethylene oxidation, Polym. Degrad. Stabil. 155 (2018) 67–83, https://doi.org/10.1016/j.polymdegradstab.2018.07.011.

[35] A.L. Forster, Z. Tsinas, M. Al-Sheikhly, Effect of irradiation and detection of long-lived polyenyl radicals in highly crystalline ultra-high molar mass polyethylene (UHMMPE) fibers, Polymers 11 (2019), https://doi.org/10.3390/polym11050924.

[36] F. Shen, H.A. Mckellop, Interaction of Oxidation and Crosslinking in Gamma-Irradiated Ultrahigh Molecular-Weight Polyethylene, 2001.

[37] J. Durant, M.S. Jahan, EPR power saturation techniques and spectral differentiation are used to isolate and simulate radical species in UHMWPE, Nucl. Instrum. Methods Phys. Res. Sect. B Beam Interact. Mater. Atoms 236 (2005) 160–165, https://doi.org/10.1016/j.nimb.2005.04.011.

[38] A.L.G. Biancolli, S. Bsoul-Haj, J.C. Douglin, A.S. Barbosa, R.R. de Sousa, O. Rodrigues, A.J.C. Lanfredi, D.R. Dekel, E.I. Santiago, High-performance radiation grafted anion-exchange membranes for fuel cell applications: effects of irradiation conditions on ETFE-based membranes properties, J. Membr. Sci. 641 (2022), https://doi.org/10.1016/j.memsci.2021.119879.

[39] M.S. Jahan, J. Durant, Investigation of the oxygen-induced radicals in ultra-high molecular weight polyethylene, Nucl. Instrum. Methods Phys. Res. Sect. B Beam Interact. Mater. Atoms 236 (2005) 166–171, https://doi.org/10.1016/j.nimb.2005.04.014.

[40] M. Mélot, Y. Ngono-Ravache, E. Balanzat, Very low temperature irradiation of aliphatic polymers: role of radical migration on the creation of stable groups (O-127), Nucl. Instrum. Methods Phys. Res. Sect. B Beam Interact. Mater. Atoms 208 (2003) 345–352, https://doi.org/10.1016/S0168-583X(03)00892-9.

[41] A. Chapiro, Radiation Chemistry of Polymeric Systems, Wiley Interscience Publishers, New York, 1962.

[42] C. Decker, F.R. Mayo, H. Richardson, Aging and degradation of polyolefins - 3. Polyethylene and ethylene-propylene copolymers, J. Polym. Sci. 1 Polym. Chem. 11 (1973) 2879–2898, https://doi.org/10.1002/pol.1973.170111110.

[43] B.J. Lyons, The effect of radiation on the solubility and other properties of high and linear low density polyethylenes, Radiat. Phys. Chem. 22 (1983) 135–153, https://doi.org/10.1016/0146-5724(83)90200-5.

[44] J.C. Randall, F.J. Zoepfl, J. Silverman, A 13C NMR study of radiation-induced long-chain branching in polyethylene, Makromol. Chem. Rapid Commun. 4 (1983) 149–157, https://doi.org/10.1002/marc.1983.030040307.

[45] T. Seguchi, N. Tamura, Mechanism of decay of alkyl radicals in irradiated polyethylene on exposure to air as studied by electron spin resonance, J. Phys. Chem. 77 (1973) 40–44, https://doi.org/10.1021/j100620a008.

[46] A. Torikai, R. Geetha, S. Nagaya, K. Fueki, Radiation-induced degradation of polyethylene: role of amorphous region in the formation of oxygenated products and the mechanical properties, Polym. Degrad. Stabil. 16 (1986) 199–212, https://doi.org/10.1016/0141-3910(86)90064-9.

[47] M. Ogasawara, Application of Pulse-Radiolysis to the Study of Polymers and Polymerization, Springer, Adv. Polymers Science, Berlin, 1993.

[48] W. Lee, K. Saito, S. Furusaki, T. Sugo, K. Makuuchi, Design of urea-permeable anion-exchange membrane by radiation-induced graft polymerization, J. Membr. Sci. 81 (1993) 295–305, https://doi.org/10.1016/0376-7388(93)85181-U.

[49] Y. Oren, I. Rubinstein, C. Linder, G. Saveliev, B. Zaltzman, E. Mirsky, O. Kedem, Modified heterogeneous anion-exchange membranes for desalination of brackish and recycled water, Environ. Eng. Sci. 19 (2002) 513–529, https://doi.org/10.1089/109287502320963472.

[50] A.L.G. Biancolli, D. Herranz, L. Wang, G. Stehlíková, R. Bance-Soualhi, J. Ponce-González, P. Ocón, E.A. Ticianelli, D.K. Whelligan, J.R. Varcoe, E.I. Santiago, ETFE-based anion-exchange membrane ionomer powders for alkaline membrane fuel cells: a first performance comparison of head-group chemistry, J. Mater. Chem. A. 6 (2018) 24330–24341, https://doi.org/10.1039/c8ta08309f.

[51] L. Wang, E. Magliocca, E.L. Cunningham, W.E. Mustain, S.D. Poynton, R. Escudero-Cid, M.M. Nasef, J. Ponce-González, R. Bance-Souahli, R.C.T. Slade, D. K. Whelligan, J.R. Varcoe, An optimised synthesis of high performance radiation-grafted anion-exchange membranes, Green Chem. 19 (2017) 831–843, https://doi.org/10.1039/c6gc02526a.

[52] A. D2765-16, Standard test methods for determination of gel content and swell ratio of crosslinked ethylene plastics, ASTM International, West Conshohocken, 2016, https://doi.org/10.1520/D2765-16.

[53] X. Cao, D. Novitski, S. Holdcroft, Visualization of hydroxide ion formation upon electrolytic water splitting in an anion exchange membrane, ACS Mater. Lett. 1 (2019) 362–366, https://doi.org/10.1021/acsmaterialslett.9b00195.

[54] J. Müller, A. Zhegur, U. Krewer, J.R. Varcoe, D.R. Dekel, Practical ex-situ technique to measure the chemical stability of anion-exchange membranes under conditions simulating the fuel cell environment, ACS Mater. Lett. 2 (2020) 168–173, https://doi.org/10.1021/acsmaterialslett.9b00418.

[55] A. Zhegur-Khais, F. Kubannek, U. Krewer, D.R. Dekel, Measuring the true hydroxide conductivity of anion exchange membranes, J. Membr. Sci. 612 (2020), 118461, https://doi.org/10.1016/j.memsci.2020.118461.

[56] N. Ziv, D.R. Dekel, A practical method for measuring the true hydroxide conductivity of anion exchange membranes, Electrochem. Commun. 88 (2018) 109–113, https://doi.org/10.1016/j.elecom.2018.01.021.

[57] A. Ashfaq, M.C. Clochard, X. Coqueret, C. Dispenza, M.S. Driscoll, P. Ulański, M. Al-Sheikhly, Polymerization reactions and modifications of polymers by ionizing radiation, Polymers 12 (2020) 1–67, https://doi.org/10.3390/polym12122877.
[58] M. Dole, in: The Radiation Chemistry of Macromolecules, vol. 3, Academic Press, New York, 1973. http://public.eblib.com/choice/publicfullrecord.aspx?P=1839542.
[59] J. Petrůj, J. Marchal, Mechanism of ketone formation in the thermooxidation and radiolytic oxidation of low density polyethylene, Radiat, Phys. Chem. 16 (1980) 27–36, https://doi.org/10.1016/0146-5724(80)90110-7.
[60] D.J. Carlsson, R. Brousseau, C. Zhang, D.M. Wiles, Polyolefin oxidation: quantification of alcohol and hydroperoxide products by nitric oxide reactions, Polym. Degrad. Stabil. 17 (1987) 303–318, https://doi.org/10.1016/0141-3910(87)90090-5.
[61] J. Lacoste, D.J. Carlsson, Gamma-, photo-, and thermally-initiated oxidation of linear low density polyethylene: a quantitative comparison of oxidation products, J. Polym. Sci. Part A Polym. Chem. 30 (1992) 493–500, https://doi.org/10.1002/pola.1992.080300316.
[62] A. Singh, Irradiation of polyethylene: some aspects of crosslinking and oxidative degradation, Radiat. Phys. Chem. 56 (1999) 375–380, https://doi.org/10.1016/S0969-806X(99)00328-X.
[63] P.J. Butiagin, The decay of free radicals in polymer media, Pure Appl. Chem. 30 (1972) 57–76, https://doi.org/10.1351/pac197230010057.
[64] J. Sohma, Radical Migration as an elementary process in degradation, Pure Appl. Chem. 53 (1983) 1595–1601, https://doi.org/10.1351/pac198355101595.
[65] R.G. Hicks, What's new in stable radical chemistry? Org. Biomol. Chem. 5 (2007) 1321–1338, https://doi.org/10.1039/b617142g.
[66] M. Hedenqvist, U.W. Gedde, Diffusion of small-molecule penetrants in semicrystalline polymers, Prog. Polym. Sci. 21 (1996) 299–333, https://doi.org/10.1016/0079-6700(95)00022-4.
[67] S. Serranti, G. Bonifazi, Techniques for Separation of Plastic Wastes, Elsevier Ltd, 2019, https://doi.org/10.1016/b978-0-08-102676-2.00002-5.
[68] R.A. Fouracre, H.M. Banford, X. Cao, H. Wang, D.J. Tedford, Radiation Effects in Polymers, 1989, pp. 469–473, https://doi.org/10.1016/b978-0-7204-0247-6.50014-7.
[69] M. Walo, G. Przybytniak, J. Sadło, Radiation-induced radicals in aliphatic poly (ester urethane)s studied by EPR spectroscopy, J. Mol. Struct. 1036 (2013) 488–493, https://doi.org/10.1016/j.molstruc.2012.12.011.
[70] Z.Y. Zhu, W.W. Gou, J.H. Chen, Q.G. Zhang, A.M. Zhu, Q.L. Liu, Crosslinked naphthalene-based triblock polymer anion exchange membranes for fuel cells, J. Membr. Sci. 636 (2021), https://doi.org/10.1016/j.memsci.2021.119569, 119569.
[71] X. Zhou, L. Wu, G. Zhang, R. Li, X. Hu, X. Chang, Y. Shen, L. Liu, N. Li, Rational design of comb-shaped poly(arylene indole piperidinium) to enhance hydroxide ion transport for H2/O2 fuel cell, J. Membr. Sci. 631 (2021), https://doi.org/10.1016/j.memsci.2021.119335.
[72] N.W.L.M. Zhang, J.L. Liu, Y.G. Wang, L.A. An, M.D. Guiver, Highly stable anion exchange membranes based on quaternized polypropylene, J. Mater. Chem. 3 (2015) 12284–12296, https://doi.org/10.1039/C5TA01420D.
[73] J. Xue, L. Liu, J. Liao, Y. Shen, N. Li, UV-crosslinking of polystyrene anion exchange membranes by azidated macromolecular crosslinker for alkaline fuel cells, J. Membr. Sci. 535 (2017) 322–330, https://doi.org/10.1016/j.memsci.2017.04.049.
[74] S. He, L. Liu, X. Wang, S. Zhang, M.D. Guiver, N. Li, Azide-assisted self-crosslinking of highly ion conductive anion exchange membranes, J. Membr. Sci. 509 (2016) 48–56, https://doi.org/10.1016/j.memsci.2016.02.045.
[75] E. Oral, A.L. Neils, K.K. Wannomae, O.K. Muratoglu, Novel active stabilization technology in highly crosslinked UHMWPEs for superior stability, Radiat. Phys. Chem. 105 (2014) 6–11, https://doi.org/10.1016/j.radphyschem.2014.05.017.
[76] C. Albano, R. Perera, P. Silva, Y. Sánchez, Characterization of irradiated PEs/PA6 blends, Polym. Bull. 57 (2006) 901–912, https://doi.org/10.1007/s00289-006-0651-y.
[77] P.S.Y.S.C. Albano, R. Perera, Characterization of gamma irradiation pes using ESR, FTIR, and DSC techniques, Polym. Bull. 51 (2003) 135–142, https://doi.org/10.1007/s00289-003-0206-4.
[78] S. Kim, P.H. Kang, Y.C. Nho, O.B. Yang, Effect of electron beam irradiation on physical properties of ultrahigh molecular weight polyethylene, J. Appl. Polym. Sci. 97 (2005) 103–116, https://doi.org/10.1002/app.21734.
[79] E. Suljovrujic, Dielectric study of post-irradiation effects in gamma-irradiated polyethylenes, Radiat, Phys. Chem. 79 (2010) 751–757, https://doi.org/10.1016/j.radphyschem.2010.02.008.
[80] E. Suljovrujic, Post-irradiation effects in polyethylenes irradiated under various atmospheres, Radiat, Phys. Chem. 89 (2013) 43–50, https://doi.org/10.1016/j.radphyschem.2013.04.003.
[81] H. Sato, M. Shimoyama, T. Kamiya, T. Amari, S. Aic, T. Ninomiya, H.W. Siesler, Y. Ozaki, Raman spectra of high-density, low-density, and linear low-density polyethylene pellets and prediction of their physical properties by multivariate data analysis, J. Appl. Polym. Sci. 86 (2002) 443–448, https://doi.org/10.1002/app.10999.
[82] S. Chan Park, H. Shinzawa, J. Qian, H. Chung, Y. Ozaki, M.A. Arnold, Improved accuracy for Raman spectroscopic determination of polyethylene property by optimization of measurement temperature and elucidation of its origin by multiple perturbation two-dimensional correlation spectroscopy, Analyst 136 (2011) 3121–3129, https://doi.org/10.1039/c1an15231a.
[83] P. Larkin, Introduction, Infrared Raman Spectrosc, 2011, pp. 1–5, https://doi.org/10.1016/b978-0-12-386984-5.10001-1.
[84] J.W.R.P. Ray, B. Amit, Polymer Grafting and Crosslinking, Wiley, New Jersey, 2009.
[85] K.A. Murray, J.E. Kennedy, B. McEvoy, O. Vrain, D. Ryan, R. Cowman, C. L. Higginbotham, The effects of high energy electron beam irradiation in air on accelerated aging and on the structure property relationships of low density polyethylene, Nucl. Instrum. Methods Phys. Res. Sect. B Beam Interact. Mater. Atoms 297 (2013) 64–74, https://doi.org/10.1016/j.nimb.2012.12.001.
[86] H. Kudoh, N. Kasai, T. Sasuga, T. Seguchi, Low temperature gamma-ray irradiation effects on polymer materials - 2. Irradiation at liquid helium temperature, Radiat. Phys. Chem. 48 (1996) 89–93, https://doi.org/10.1016/0969-806X(95)00432-W.
[87] R. Epsztein, E. Shaulsky, M. Qin, M. Elimelech, Activation behavior for ion permeation in ion-exchange membranes: role of ion dehydration in selective transport, J. Membr. Sci. 580 (2019) 316–326, https://doi.org/10.1016/j.memsci.2019.02.009.
[88] M.M. Hossain, L. Wu, X. Liang, Z. Yang, J. Hou, T. Xu, Anion exchange membrane crosslinked in the easiest way stands out for fuel cells, J. Power Sources 390 (2018) 234–241, https://doi.org/10.1016/j.jpowsour.2018.04.064.
[89] C. Hu, Q. Zhang, H. Wu, X. Deng, Q. Yang, P. Liu, Y. Hong, A. Zhu, Q. Liu, Dual hydrophobic modifications toward anion exchange membranes with both high ion conductivity and excellent dimensional stability, J. Membr. Sci. 595 (2020), 117521, https://doi.org/10.1016/j.memsci.2019.117521.
[90] M. Mamlouk, K. Scott, Effect of anion functional groups on the conductivity and performance of anion exchange polymer membrane fuel cells, J. Power Sources 211 (2012) 140–146, https://doi.org/10.1016/j.jpowsour.2012.03.100.
[91] L. Gubler, Polymer design strategies for radiation-grafted fuel cell membranes, Adv. Energy Mater. 4 (2014), 1300827, https://doi.org/10.1002/aenm.201300827.
[92] A. Oshima, S. Ikeda, T. Seguchi, Y. Tabata, Temperature effect on radiation induced reactions in ethylene and tetrafluoroethylene copolymer (ETFE), Radiat. Phys. Chem. 50 (1997) 519–522, https://doi.org/10.1016/S0969-806X(97)00080-7.